Ameera F. Mohammad, Aya A-H. I. Mourad, Jawad Mustafa, Ali H. Al-Marzouqi*, Muftah H. El-Naas, Mohamed H. Al-Marzouqi, Fadi Alnaimat, Mabruk I. Suleiman, Mohamed Al Musharfy and Tommy Firmansyah

Computational fluid dynamics simulation of an Inert Particles Spouted Bed Reactor (IPSBR) system

https://doi.org/10.1515/ijcre-2020-0025
Received February 2, 2020; accepted May 3, 2020; published online June 25, 2020

Abstract: A novel system for contacting gases and liquids, suitable for many applications involving gas–liquid contact such as CO_2 capture and brine desalination, has been simulated and experimentally validated. The system comprises a vertical vessel with gas and liquid ports and inert particles that enhance mixing and provide a high gas–liquid interfacial area. A low gas flow rate was statistically demonstrated and experimentally verified to be the optimum condition for CO_2 capture and brine desalination; however, the gas velocity can have a considerable effect on the motion of inert particles inside the reactor. Uniform particles motion ensures good mixing within the reactor and hence efficient absorption and stripping process. A computational fluid dynamics (CFD) model, namely Eulerian model, presented in this paper, will help demonstrate the effect of mixing particles at specific conditions on the gas and liquid velocities inside the reactor, gas and liquid volume distribution through reactor, and eddy viscosities stresses of the mixing particles. A mesh-independent study was conducted to demonstrate the independency of mesh structure and size on the output responses. A quasi-steady state was attained to ensure the stability and feasibility of the selected model. The assembled model exhibits remarkable applicability in determining the optimum mixing particles densities, volume ratios, and sizes to ensure best velocity distribution and gas spreading inside the reactor and accordingly enhance the associated chemical reactions.

Keywords: CFD simulation; Eulerian model; gas-liquid reactor; inert mixing particles.

***Corresponding author: Ali H. Al-Marzouqi,** College of Engineering, UAE University, P.O. Box: 15551, Al Ain, United Arab Emirates, E-mail: hassana@uaeu.ac.ae

Ameera F. Mohammad, Jawad Mustafa, Mohamed H. Al-Marzouqi and Fadi Alnaimat: College of Engineering, UAE University, Al Ain, United Arab Emirates

Aya A-H. I. Mourad: College of Engineering, UAE University, Al Ain, United Arab Emirates; Academic Support Department, Abu Dhabi Polytechnic, Institute of Applied Technology, Abu Dhabi, United Arab Emirates

Muftah H. El-Naas: Gas Processing Center, College of Engineering, Qatar University, Doha, Qatar

Mabruk I. Suleiman, Mohamed Al Musharfy and Tommy Firmansyah: Research Centre Division, ADNOC Refining, Abu Dhabi, United Arab Emirates

1 Introduction

Gas–liquid reactors, particularly bubble column reactors, are very important and play a significant role in many chemical processes. In a bubble column reactor, a discontinuous gas phase in the form of bubbles is developed at the bottom of a vessel through an orifice and moves relative to the continuous liquid phase, exchanging mass, momentum, and energy. Bubble reactors are excellent reactors for processes that require a large interfacial area for gas–liquid mass transfer and large liquid holdup that is favorable for slow liquid phase reactions (Charpentier 1981). The distinct advantages of bubble columns over other gas–liquid reactors are their simple design and construction, low operation and maintenance costs, excellent heat and mass transfer characteristics as well as temperature control, absence of moving parts, and high mixing ability (El-Naas 2017; Gemello et al. 2018). Bubble columns are widely used in many applications in the bioprocessing industry such as oxidation, hydrogenation, Fischer–Tropsch synthesis, chemicals production, coal liquefaction, and fermentation (Gemello et al. 2018; McClure et al. 2015). However, the performance of the bubble column is influenced by a few parameters such as liquid-phase, back-mixing, bubble-size distributions, bubble–bubble interactions in the turbulent flow regimes, and bubble rise velocities. In addition, modeling such reactors is difficult, although it appears to be simple. The lack of complete understanding of the fluid dynamics and the characteristics of mass transfer under practical industrial conditions makes it difficult to scale-up and improve its

performance (Lemoine et al. 2008). The hydrodynamic studies for gas–liquid bubble columns have been conducted based on computational fluid dynamics (CFD) (Dhotre et al. 2004; Pflleger and Becker 2001; Pfleger et al. 1999; Pourtousi et al. 2014) for exhibiting flow features and predicting the flow pattern of bubble columns. Pfleger and Becker (2001) have examined the liquid phase measurement considering the local liquid phase velocities and gas volume fraction in 3-D bubble column reactors. They employed a dynamic Eulerian–Eulerian 2 phase model and standard k–ε turbulence model. In their work, Pfleger and Gomes (1999) examined the performance of an air–water system with low gas void fraction to develop a laminar and turbulent model. The laminar model exhibits a chaotic behavior and cannot produce the harmonic oscillation observed in the experiments. However, a turbulent model can demonstrate this performance. A transient 2-D axisymmetric model has been discussed by Sanyal et al. (1999) to validate a laboratory-scale cylindrical air–water bubble column, run under bubbly flow and churn turbulent conditions. FLUENT software has been utilized to conduct numerical simulation and compare the findings obtained from the Eulerian multiphase model and algebraic slip mixture model. Good quantitative agreement was observed between the experimental data and simulations. The results show that, the simple 2-D axisymmetric model can be utilized to accurately estimate the overall flow pattern and gas holdup distributions. In their review, Pourtousi et al. (2014) show suitable interfacial forces, turbulent dispersion models, virtual mass and turbulence models, Reynolds stress model, and large eddy simulation to predict flow pattern inside the bubble column using Eulerian–Eulerian model. The influence of various interfacial forces and turbulence models on gas–liquid velocity and gas hold-up in bubble column is considered. The numerical study of the bubble column indicated that bubble size can significantly influence the findings. Dhotre and Ekambara (2004) have simulated the impact of the sparger design and height to diameter ratio and radial gas hold-up profiles. Three different gas–liquid systems have been simulated. Buwa et al. (2002) examined both experimentally and numerically the impact of gas velocity sparger design and coalescence suppressing additives on the dynamics of gas–liquid flow in a rectangular bubble column. In this study, the hydrodynamics of an Inert Particles Spouted Bed Reactor (IPSBR) that can provide excellent gas–liquid contact, high performance efficiency, and can be easily scaled-up has been investigated (El-Naas 2017). The system is suitable for numerous gas–liquid contact applications and was previously evaluated for CO_2 capture and brine desalination (El-Naas 2017). Therefore, this paper presents a CFD representation for the flow dynamics and particle movements in the IPSBR. The mixture of fluid and Eulerian model are implemented to simulate the performance of multiphase flow with mixing particles inside 2-D gas–liquid contactor system.

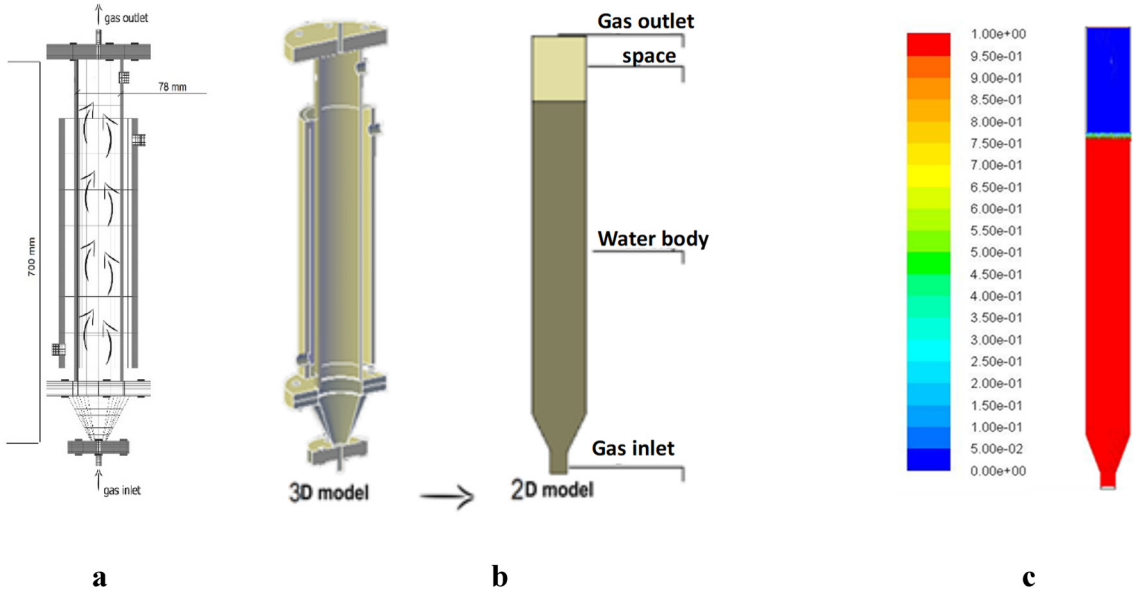

Figure 1: Gas–liquid contactor system with major dimensions and flow path for gas into liquid filled reactor (semi-batch mode), (b) gas–liquid contactor system with 3D side view and simulated 2D model, (c) contours of volume fraction of water at time flow of 0 s.

2 Simulation set-up

The geometry and mesh of the gas–liquid contactor system were established using Gambit 2.4.6 software. The geometry and mesh were exported to ANSYS Fluent 15 to simulate the flow of gas into the system under a semi-batch mode. The two-dimensional flow domain was constructed for air to flow in liquid water, as shown in Figure 1a,b. The geometry and mesh for the reactor system is in the semi-batch mode. The geometry of the gas–liquid contactor system was established in 2D with mesh of unstructured elements and a triangular form, using advanced size function on curvature and high smoothing with a curvature normal angle of 18.0°, minimum size of 5×10^{-4} m, maximum size of 5×10^{-3} m, and growth rate of 1.20. Computational grid and mesh structure for conical and cylindrical part of contactor system is illustrated in Figure 2. The mesh setup comprises four sections, namely, gas inlet, gas outlet, water body, and space. Air flows in through a conical region through an orifice with a diameter of 0.002 m to a cylindrical region of the contactor system; air then flows out through the gas outlet section on the top of the system. The system initially is filled with 3 L of water with air space at the top of the reactor that provides the ability for increasing the water head after gas starts flowing, as shown in Figure 1c. Table 1 lists the major variables for mesh characteristics and quality evaluation. From these values, the minimum orthogonal quality and maximum aspect ratio indicate a high quality for the mesh structure.

3 Numerical simulation

In the present work, the flow in the bubble column reactor was modeled using Eulerian multiphase and mixture of fluid approaches, which were simulated using the FLUENT software assuming axisymmetry. Although both models are used to predict multiphase flows, there are fundamental differences between them, which are outlined here. The temperature variation is assumed to be negligible and hence the model is considered isothermal. Further, the liquid phase is assumed to be incompressible and the gas phase to have constant properties. Bubbles are generated at the bottom of the reactor base through 0.002 m diameter spherical orifice, with equal size bubbles. The coalescence and breakage properties are neglected. The sum of the volume fraction of two phases is taken as unity. A single pressure field is assumed to be shared for two phases and no mass is exchanged between the two phases. The primary phase is considered to be water, and the secondary phase, air. Moreover, no slip boundary conditions were implemented at all the impermeable walls and atmospheric pressure was imposed at the top of the column.

3.1 Eulerian multiphase model

The Eulerian method is preferred for high gas holdup and churn turbulent flows (Zhang 2007). In the Eulerian two-fluid approach, the different phases are treated mathematically as interpenetrating continua. The conservation equations for mass, momentum, and energy for each of the individual phases is derived by ensemble averaging the local instantaneous balances for each of the phases (Anderson and Jackson 1967). The Eulerian–Eulerian approach is based on the assumption that the dispersed and continuous phases are interpenetrating continua (Sanyal et al. 1999). This approach is useful for solving multiphase and turbulent flow. Both the liquid and gas phases are considered to be two distinct phases, interacting with each other in the computational domain. The multiphase flow in the bubble column was described using the concept of phase volume fractions. A separate volume fraction equation was solved in each computational cell to determine the volume fraction of the liquid and gas phases in that cell. Inter-phase momentum transfer terms were implemented into the respective phase's momentum balance equations to couple between the motion of the dispersed and continuous phases. In addition, momentum transfer between the phases is modeled through a drag term, which is a function of the local slip velocity between the phases. A characteristic diameter is assigned to the dispersed phase gas bubbles, and a drag formulation based on a single sphere settling in an infinite medium is used. Turbulence in either phase is modeled separately.

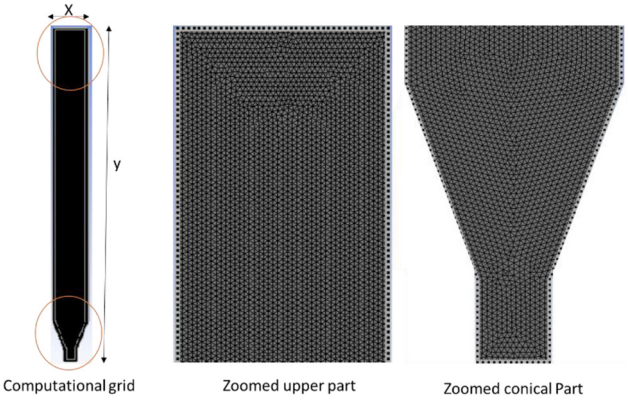

Figure 2: Computational grid and mesh structure for conical and cylindrical part of contactor system.

The details of the governing equations used in the simulations are shown below (Sanyal et al. 1999).

3.1.1 Continuity equation

$$\frac{\partial}{\partial t}(\alpha_k \rho_k) + \nabla.\left(\alpha_k \rho_k \vec{v}_m\right) = \sum_{p=1}^{n} \dot{m}_{pk} \tag{1}$$

3.1.2 Momentum equation

$$\frac{\partial}{\partial t}\left(\alpha_k \rho_m \vec{v}_m\right) + \nabla.\left(\alpha_k \rho_k \vec{v}_m \vec{v}_m\right) = -\alpha_k \nabla .\bar{\bar{\tau}}_k + \sum_{p=1}^{n}\left(\vec{R}_{pk} + \dot{m}_{pk}\vec{v}_k\right) + \alpha_k \rho_k\left(\vec{F}_k + \vec{F}_{lift,k} + \vec{F}_{\text{virtual mass},\,k}\right) \tag{2}$$

where τ_k is the kth phase stress-strain tensor, whose components are given as follows:

$$\tau_{k,ij} = \alpha_k \mu_k\left(\frac{\partial v_{k,j}}{\partial x_j} + \frac{\partial v_{k,j}}{\partial x_i}\right) \frac{-2}{3}\alpha_k \mu_k \delta_{ij}\frac{\partial v_{k,i}}{\partial x_i} \tag{3}$$

The fourth term on the right-hand side of Eq. (2) rep resents the interphase drag term. The inter-phase exchange forces are expressed as follows:

Table 1: Mesh characteristics and quality variables.

Minimum orthogonal quality	8.88346e-01
Maximum aspect ratio	3.14807
Maximum ortho skew	0.818406
Nodes Counts	18,311
Elements Counts	32,871
Wedges Counts	10
Minimum volume in m^3	8.515089e-07
Maximum volume in m^3	2.283481e-06
Total volume in m^3	5.692905e-02
Maximum face area in m^2	2.559799e-03
Minimum face area in m^2	1.099246e-03

Table 2: Inter particle specifications (El-Naas 2017).

Material	Poly methyl methacrylate (PMMA)
Average size	13 mm
Average weight	0.511 g/particle
Wet density	1.022 g/cm^3
Volume	0.5 cm^3/particle
Surface area	4.92 cm^2/particle
Sphericity	0.62

$$\vec{R}_{pk} = K_{pk}\left(\vec{v}_q - \vec{v}_k\right) \tag{4}$$

where K_{pk} being the momentum exchange coefficient between the pth and the kth phases.

3.1.3 Mixing particles

The effect of inert particle on CO_2 capture, ion removal, and residence time distribution in the IPSBR was examined experimentally in previous studies (El-Naas et al. 2017; Ibrahim et al. 2019). Inert particles create a circular motion within the vessel, enhancing mixing and providing high gas–liquid interfacial area for effective mass transfer. The inert particles comprises plastic (poly methyl methacrylate) with an average particle size of 0.013 m and a density of 1,020 kg/m^3. The specifications of the inert particles employed in the experiments conducted in the previous work (El-Naas et al. 2017) are listed in Table 2. Particles with an average diameter of 0.013 m provided a relatively uniform movement and excellent mixing within the reactor vessel. In the DPM, the trajectory of the

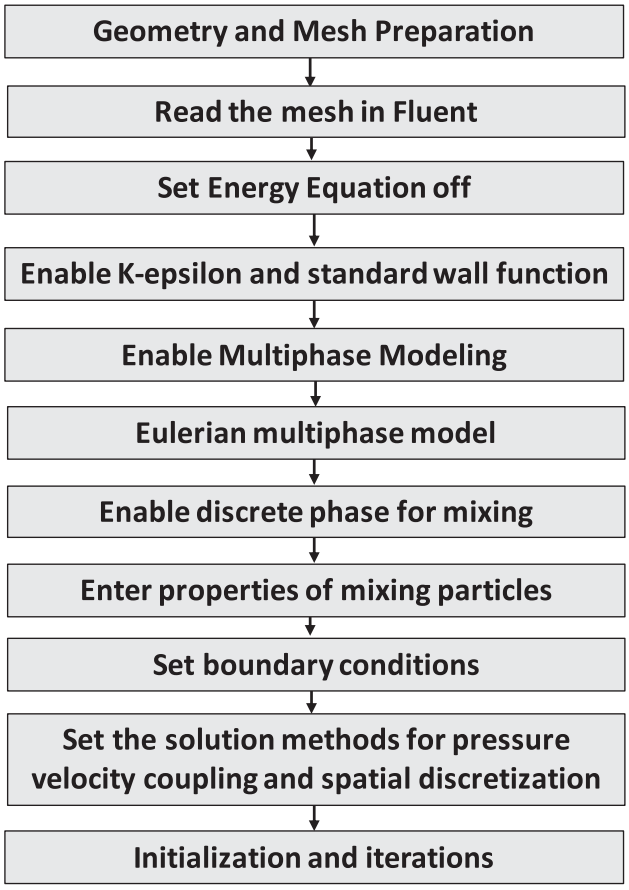

Figure 3: Eulerian model's methodology structure.

particles was tracked using the Newtonian equation of motion. Considering particle inertia and force balance, the Newtonian equation of motion is as follows (Zhang et al. 2018):

$$\frac{\partial v_p}{\partial t} = f_D\left(v - v_p\right) + \frac{g\left(\rho_p - \rho\right)}{\rho_p} + f \tag{5}$$

where $f_D(v–v_p)$ is the drag force per unit particle mass and

$$f_D = \frac{3\mu C_D Re}{4\rho_p d_p^2} \tag{6}$$

where v is the fluid phase velocity, v_p the particle velocity, μ is the molecular viscosity of the fluid, ρ is the fluid density, ρ_p the density of the particle, and dp is the particle diameter. Re is the relative Reynolds number, which is defined as

$$R_e = \frac{\rho d_p \left|v_p - v\right|}{\mu} \tag{7}$$

The drag coefficient, C_D can be defined as:

$$C_D = a_1 + \frac{a_2}{R_e} + \frac{a_3}{R_e^2} \tag{8}$$

where a_1, a_2, and a_3 are constants that can be applied for smooth spherical particles over several ranges of Re.

Equation (5) includes a force of gravity on the particle that is equal to 9.81 m/s^2.

3.2 Numerical methodology

The models were used to investigate the hydrodynamic flow behavior in an existing system comprising a stainless steel cylindrical vessel with an internal diameter of 0.078 m; height, 0.700 m; and a total working volume, 3,000 ml. The simulations were conducted under transient and gravitational acceleration conditions. The realizable k–ε model helps consider the turbulence effects of the flow of gas through water. Each model has been run in a double precision mode to increase the accuracy of the calculation. The momentum and pressure equations were solved using the phase-coupled simple scheme with volume fractions. The gradient was calculated using least squares cell based method (Patankar 1980). A first order upwind scheme is used to solve the momentum and turbulence equations (Kartushinsky 2016; Li et al. 2009, 2016). The pressure and momentum under relaxation factors are set as 0.7. The equations are then solved in a segregated, iterative fashion for increasing time steps. At each time step of 0.001, with an initial guess for air volume fraction of 0 in the primary phase, the numerical simulation was conducted in a 2D rectangular column with a width of 0.0778 m and height 0.850 m. The column was partially filled with water; then, at time t = 0.0 s, air was injected through the orifice at a velocity of 1 m/s. The numerical models were solved using the numerical solver Fluent based on a finite volume method. A hybrid initialization method was used for solution initialization. A time step (t = 0–10 s) for flow was tested for the semi-batch mode with and without mixing particles. For each time step, the convergence criteria for the sum of normalized residues were fixed at 10^{-3} and 20 iterations per time step were satisfactory. Figure 3 shows the general structure for Eulerian model methodology.

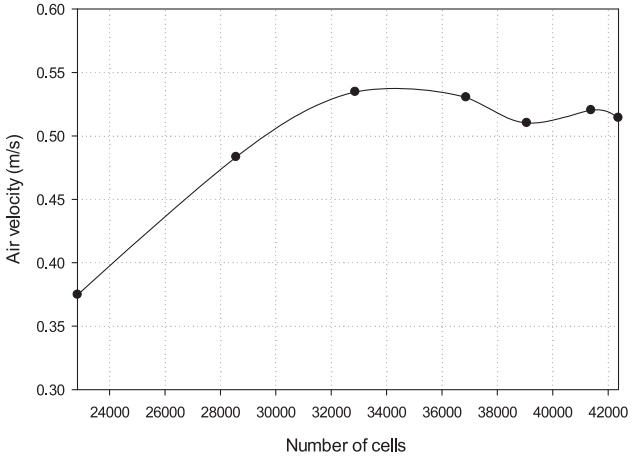

Figure 4: Mesh-independent study for air velocity in the contact system at specific flow time and distance from the gas inlet based on transient simulation.

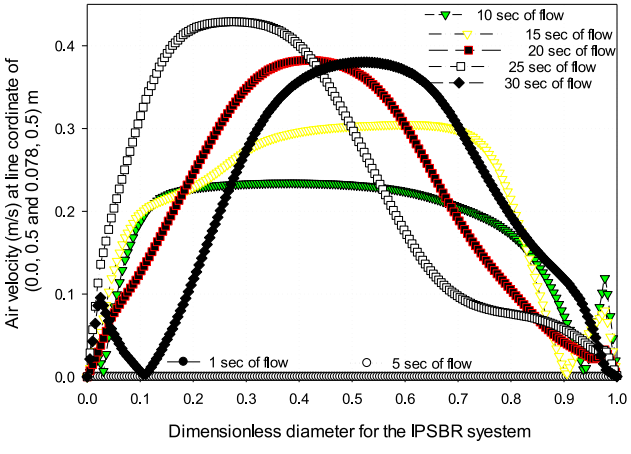

Figure 5: Quasi-steady state investigation for semi-batch mode at different flow times (1–30 s) for gas velocity of 1 m/s and without mixing particles.

4 Results and discussion

4.1 Mesh independent study

The computational accuracy of CFD simulation is correlative to the number of mesh and time step. To obtain a mesh independent solution, an intensive mesh study was conducted as shown in Figure 4. All simulations are converged using the defined convergence criterion. Seven different size meshes were tested, including 22,845, 28,568, 32,871, 36,112, 39,068, 41,386, and 42,372, with mesh size starting from 0.0022 and ending by 0.0016, respectively. A mesh study is only possible if the solution is independent of the time step and vice versa. This circumstance was considered and the mesh study was conducted with sufficiently small time steps. The study is conducted by investigating the air volume fraction as demonstrated in Figure 4, The convergence for air velocity was reached at mesh size of 0.0016 (corresponding to 42,372 cells) only around 1% different than the previous mesh size (0.0017 corresponding to 41,386 cells). The solution with its clear oscillation trend was found to be mesh-independent and there were no significant differences between the last four mesh sizes, particularly between the results of the 0.0019 and 0.0016 mesh sizes. Therefore, owing to the calculation speed and efficiency, the 0.0020 grid size which provides 2.6% difference from the finest tested mesh, would be acceptable and was applied in further 2D column tests.

4.2 Quasi-steady state study

A quai-steady state test has been conducted to specify the accurate time at which the results of bubble column should be recorded. Evidently, Figures 5, 6 show that the velocity of the air increases with time for 25 s. However, a drop in the air velocity is observed at 30 s. Therefore, the optimum time at which the results should be recorded is 20 s. The contours of air velocity of 1 m/s at 1, 5, 10, 15, 20, 25, and 30 s until the quasi-steady state is attained is shown in Figure 6. The air velocity distribution in the column is similar throughout the column for 20, 25, and 30 s, indicats that the column has achieved the quasi-steady state. Superficial air velocity plays an important role in governing the flow field in a bubble column. It is expected that with an increase in superficial air velocity, flow structures become more complex and bubble collision and breakup increases. Therefore, a further study will be carried out to investigate the effect of different superficial air velocities on the variation of flow patterns. Moreover, 3D models are still needed to provide sufficient representations of the behavior of these flow patterns.

4.3 Contour results from CFD study

Figure 7 shows a few results for the Elurian model through the contours of air velocity, water velocitiy, air volume fraction, water volume fraction, and Eddy viscosity for the semi-batch mode with mixing particles at gas velocity 1 m/s following 20 s of flow. The effect of mixing particles is shown in Figure 8, where the path lines indicate the minimization of the stagnant zones inside the reactor.

4.4 Gas–liquid time-averaged velocity distribution

The time-averaged velocity distribution for air and liquid has been studied and results are demonstrated in Figure 9a, b. All data have been extracted at a height

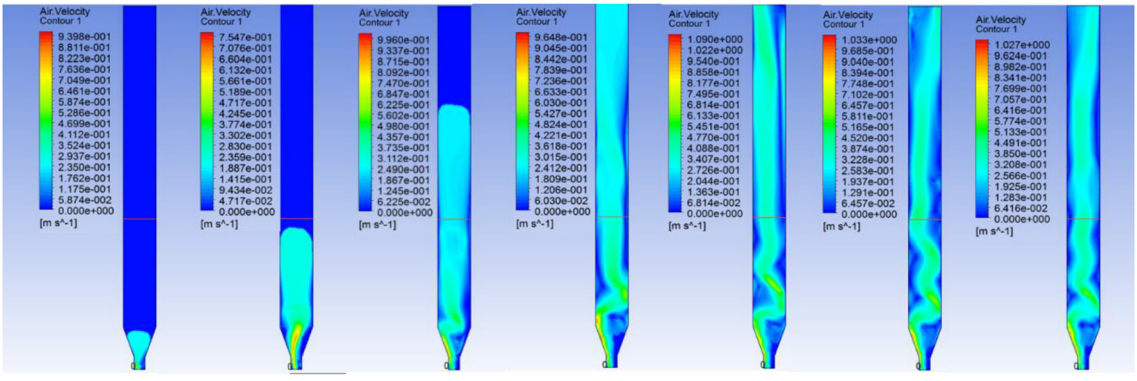

Figure 6: Air velocity contours at (a) 0, (b) 5 (c) 10, (d) 15, (e) 20, (f) 25, (g) 30 s of flow for gas velocity of 1 m/s and without mixing particles.

of 50 cm from the gas inlet after the transient state reached statistically steady state. The readings at 25 and 30 s time intervals have been averaged. The error bar reflects the repeatability of the results. The standard deviation is in the range of 0.005631 to 0.0145. Figure 9a shows that the averaged-time velocity of the air is maximum at the center of the cross-section and reduces on both sides till it reaches zero at the wall. A different pattern for the air velocity is observed when including the mixing particles. The averaged-time velocity is distributed along the cross section without showing a peak at the center as in the case of no particles. Homogeneous distribution of mixture's velocity over reactor cross section and reduction in velocity magnitude if compared to the peak value of the case of no particles are due to variation of the liquid velocity, where the fluid circulates at different intensity along the column. Further, owing to the variation of the circulation velocity, the momentum exchange results in distribution of kinetic energy for which the flow pattern and gas holdup will radically vary. In addition, increasing the liquid velocity decreases the gas holdup. The bubbles are fast driven by the liquid. The residence time of the bubbles decreases with the liquid velocity, and hence, the gas holdup is likely to decrease. In addition, an evident increase in the gas holdup inside the reactor is observed as particles are added; in this case, the liquid recirculation tends to move gas toward the right of the column. Furthermore, there is an increment in the gas holdup near the riser wall. The reason for this is that the larger sized liquid circulation at the riser bottom tends to move the gas towards the wall. Gas hold-up profile gives a prediction to pressure variation and thus liquid recirculation. Liquid recirculation has significant effect on mixing and hence heat and mass transfer predictions of radial gas hold up. All of this would lead to better understanding of this phenomenon to scale-up the bubble column.

In gas–liquid bubble columns, the velocity of liquid varies with time and location in the column.

The radial velocity profiles, from 2D simulations, of liquid phase from 0 to 0.08 m and at a height of 0.500 m from the gas inlet is shown in Figure 9b. For no particles, the averaged-time liquid velocity increases from zero at the wall surface to the free stream velocity away from the surface under a no-slip boundary condition to create a parabola as shown in Figure 9b. However, by using the particles, the water velocity sharply decreases along the radial axis and a uniform distribution along the axis and almost zero velocity at wall are illustrated. These observations reflect the significant and beneficial effect of introducing the particles in the bubble column. It is worth mentioning that using mixing particles will increase the overall average velocity inside the reactor, and hence affect the velocity profile of the gas and liquid. Still, in this study, low volume fraction of mixing particles is used and accordingly minimum effect on velocity profile is expected. However, the dominant effect on velocity profile, which is

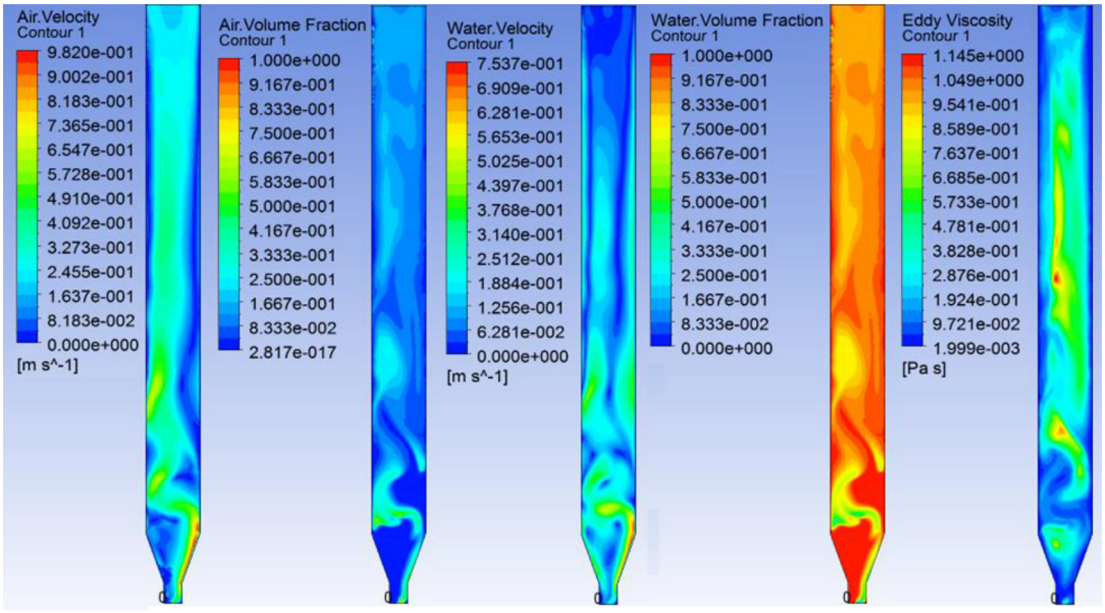

Figure 7: Eulerian model contours of gas and liquid velocities and volume fractions and eddy viscosity for the semi-batch mode with mixing particles at gas velocity of 1 m/s after 20 s of flow.

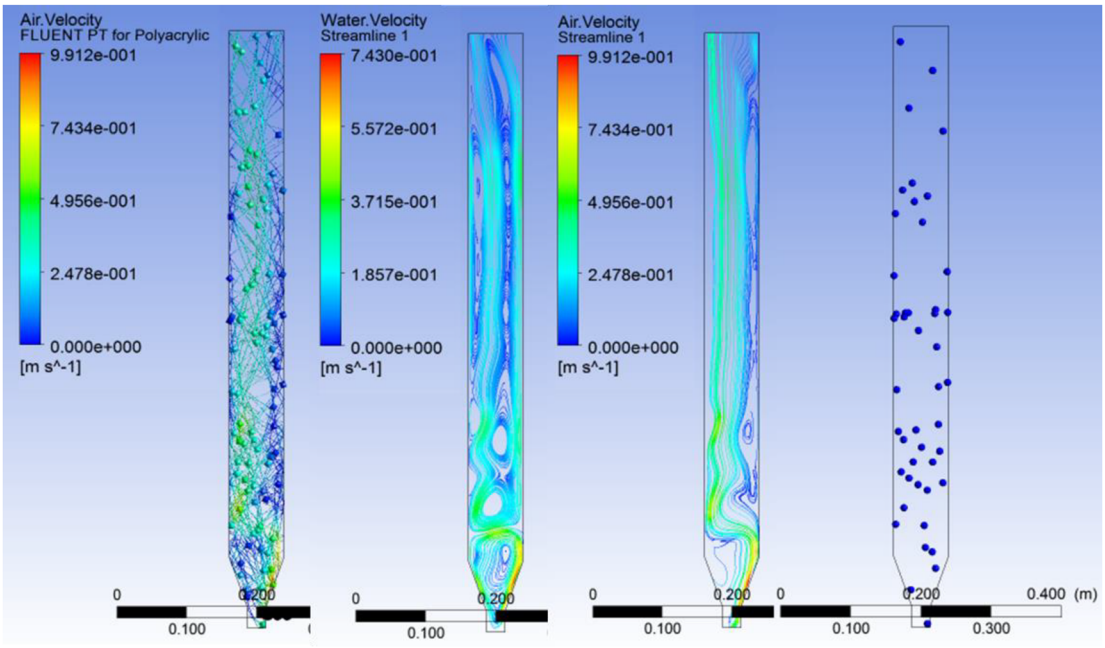

Figure 8: Particles distribution and path lines within gas and liquid velocity contours for the semi-batch mode with mixing particles at gas velocity of 1 m/s after 20 s of flow.

the changing of the average velocity or the effect of mixing particles, will be investigated in a future study.

4.5 Gas–liquid time-averaged volume fraction

Near the wall of the reactor, there is a significant difference in the value of averaged-time air fraction with and without the particles, as illustrated in Figure 9c. Without the particles, air fraction is almost zero and once the particles are added, it increased rapidly to approximately 0.2–0.3 at reactor wall. Moreover, instead of the air concentration around the centerline of the reactor when particles are not mixed, more distribution is observed over the radial coordinate when particles are mixed, and hence, more gas is spread among the reactor. Accordingly, significant improvement of mixing for the two phases is achieved, hence, increasing the mass and heat transfer.

Adding particles enhance the mixing between the water and the air, as shown in Figure 9d. The averaged-time fraction of the water at the wall for no particles is almost 1.0, which indicates that there is no proper mixing between the air and the water. However, in the presence of particles, the fraction of the water declines and that of the air increases. Figure 9c, d displays the averaged-time values at 25 and 30 s. The error bar shown in the figure reflects the accuracy and reproducibility of the results.

4.6 Time-averaged eddy viscosity study

Figure 9e illustrates that, adding particles increases significantly the eddy viscosities. This is also because an increase in the intensity of the circulation along the column axis varies with energy distribution. As for fluid velocity and volume fraction, the average values have been recorded for the reading at 25 and 30 s. The energy distribution is a function of the phase physical properties. The velocity in the core region of the column is higher than that observed at other radial positions because of the reduction in interfacial stress between the wall of the column and the liquid, and accordingly the fluid, develop circular pattern at different intensities along the column. Similarly, because of the difference between the circulation velocities, the momentum exchange results in a distribution of kinetic energy for which the flow pattern and gas holdup will radically vary.

4.7 Wall shear stress

Figure 10a, b shows the shear wall stress along dimensionless radial position at a superficial gas velocity of 1 m/s

with and without mixing particles. The dimensionless coordinate at the *x*-axis represents the distance from the wall divided by the whole diameter of 0.0778 m, all the results are taken at height of 50 cm from gas inlet. Figure 10a illustrates the change in wall shear stress in the region from 0 to 0.020. As might be expected, it is very clear from the data that the water wall shear stress with mixing particles is less than that of the non-mixing particles. As shown from the figure, the highest value with mixing particles reached almost 0.42 Pa compared with 0.78 Pa for the non-mixing particles. This is because adding particles enhances the eddy viscosities and circulation near the wall as mentioned before in section 4.6. As an overall trend, the shear stress of water with and without mixing particles remains almost stable near the wall from 0.000 to 0.020. This is due to the no-slip boundary condition, where the fluid which is mostly water will have almost a zero velocity relative to the boundary. The effect of adding mixing particle on air shear stress near the wall from 0.96 to 1 is shown in Figure 10b. The results reveal that after adding mixing particle, the air shear stress decreases rapidly from 2.5×10^{-5} Pa to a value of approximately 1.57×10^{-5} Pa , at which the stress enters a period of stability. It can be noticed that the air shear stress without mixing particle is not constant, because the concentration of air near the wall is negligible and any change in the distance from the wall will affect the stress as the intensity of air will increase. With mixing particle, there is a good distribution of air near to the wall and hence the shear stress is almost the same. In summary, results from the above shear stress analysis showed that by adding particles, the water and air wall shear stresses reduced to almost 46 and 37%, receptively.

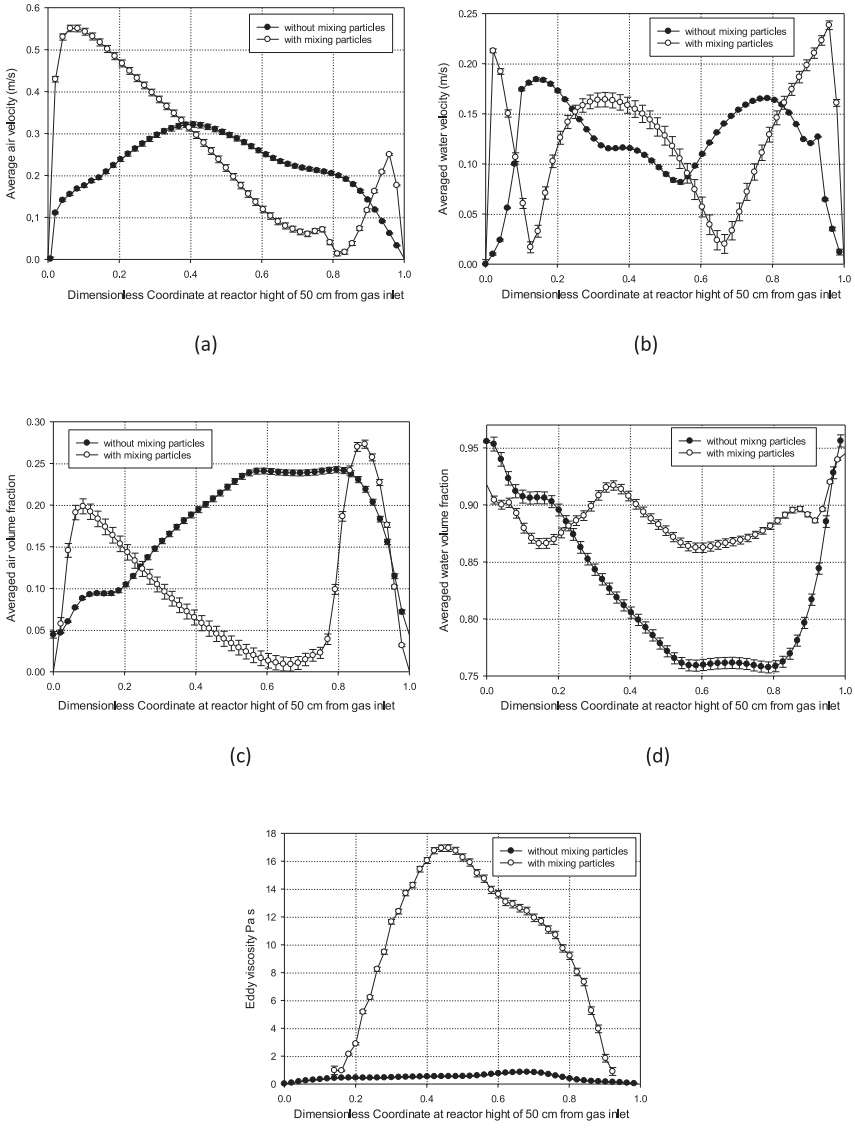

Figure 9: (a) averaged air velocity, (b) averaged liquid velocity, (c) averaged air volume fraction, (d) averaged liquid volume fraction and (e) averaged eddy viscosities for the dimensionless coordinate of the reactor system at high of 50 cm from the gas inlet.

4.8 Interfacial area

The interfacial area concentration is one of the most essential parameters for bubble column reactors. It is an important factor in determining the mass-transfer coefficient. Table 3 shows the interfacial area concentrations with and without mixing particles at different elevations. The readings were obtained at flow time of 30 s, 0.002 m orifice diameter, and gas velocity of 1 m/s. The data show that the higher interfacial area concentrations are observed at the default interior, where the bubbles were produced in the higher turbulence region, increasing the overall intensity of bubbles. Also, the interfacial area concentration was higher at the wall than at the outlet. This is because the large bubbles were broken up while moving from the center to the outlet. It is very important to note that the interfacial area concentration increased by 26.34% with mixing particles. The enhancement is due to the improvement in surface area and the chances of collisions. The contours of the interfacial area concentration for air bubbles is illustrated in Figure 11.

Table 3: Interfacial area concentrations with and without mixing particles at different elevations and 30 s flow time.

Interfacial area concentration (m^2/m^3)	With mixing particles	Without mixing particles
Default-interior	0.54966336	0.40521795
Inlet	9.9999997e-05	9.9999997e-05
Outlet	0.00044941471	0.00059999997
Wall	0.0042241924	0.0024326392
Total	0.55443698	0.40835059

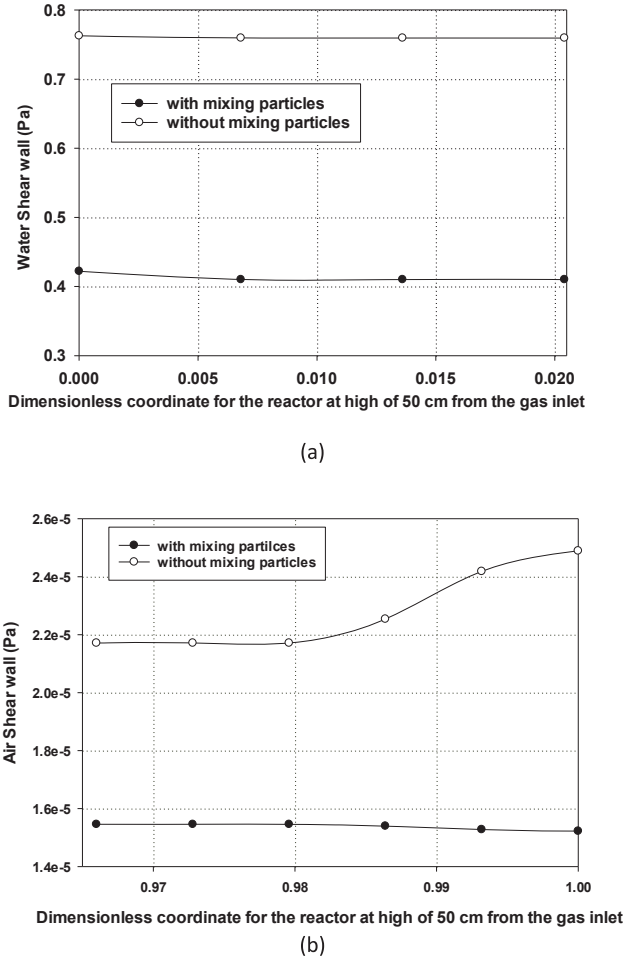

Figure 10: (a) water wall shear stress versus normalized distance from the wall and (b) air wall shear stress versus normalized distance from the wall.

5 Experimental set-up and CFD validation

For the validation of CFD simulation, a laboratory-scale IPSBR was used. Its geometry is consistent with the

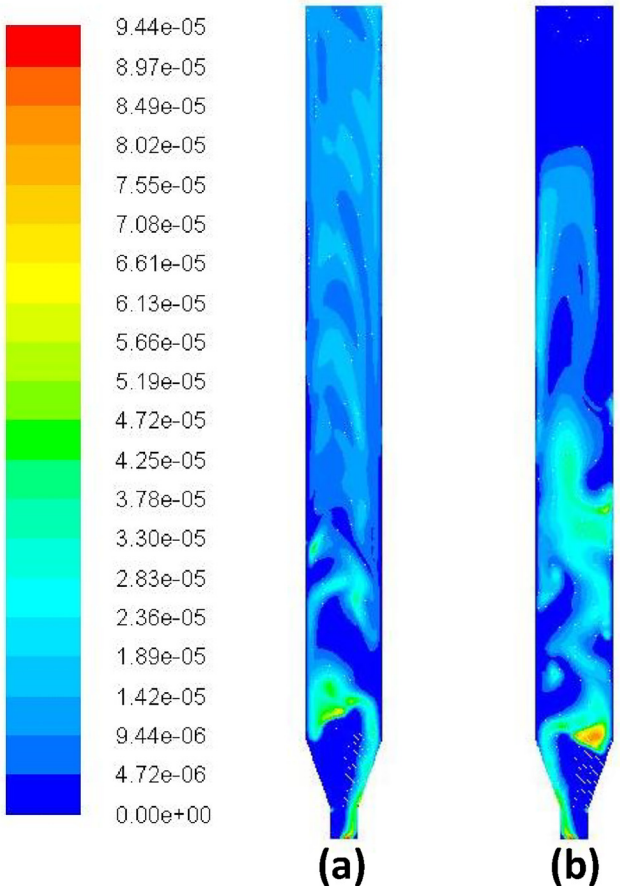

Figure 11: Contours of interfacial area concentration (m^2/m^3) for air bubbles (a) with mixing particles and (b) without mixing particles.

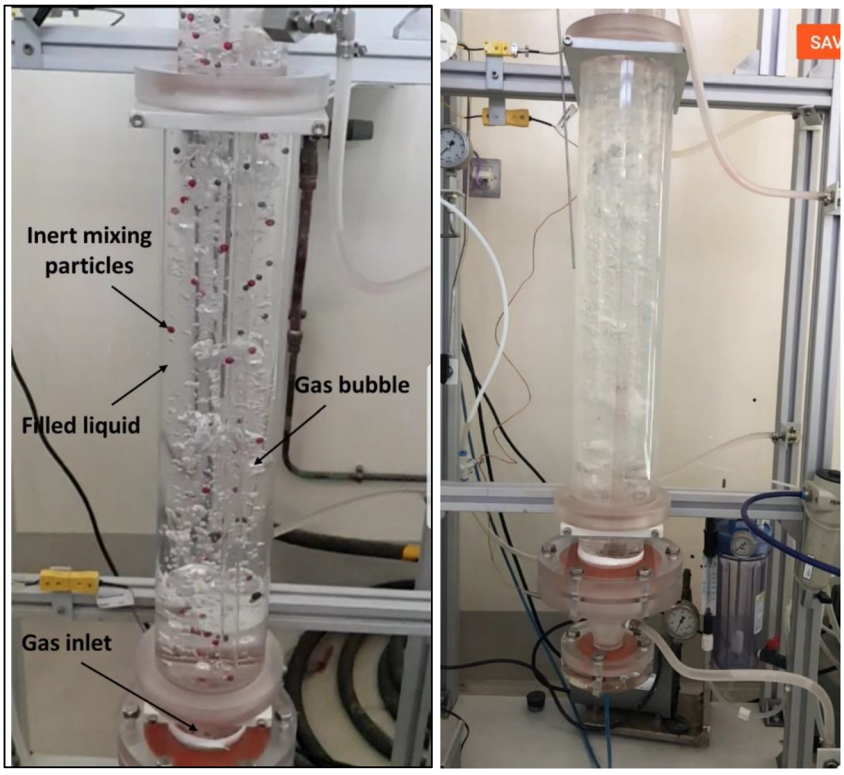

Figure 12: A laboratory-scale bubble column reactor with internal diameter of 82 mm and total high of 965 mm and gas orifice diameter of 2 mm with (a) inert mixing particles and (b) without mixing particles.

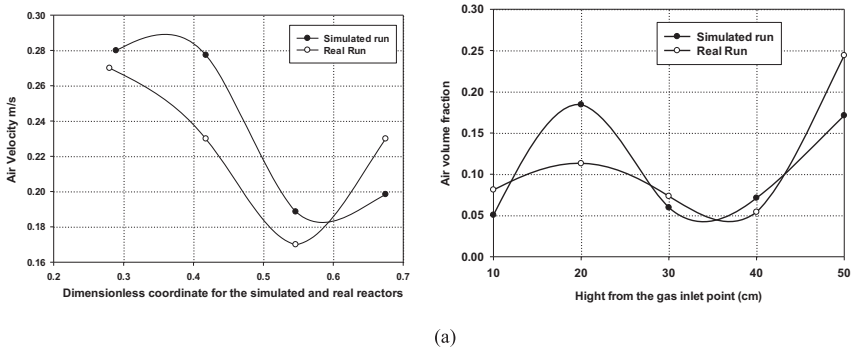

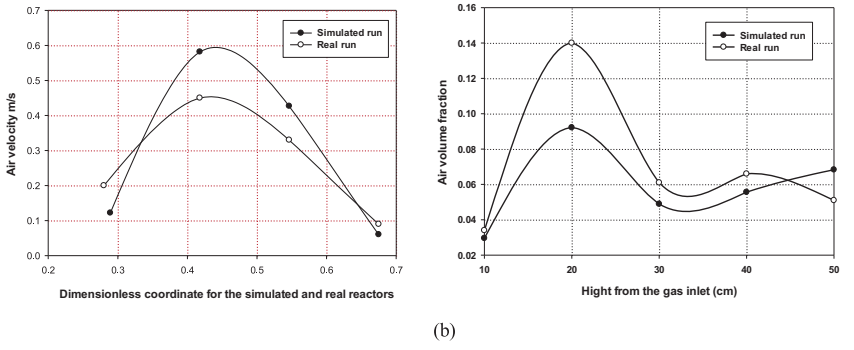

Figure 13: Experimental and simulation results at certain points for air velocity and air volume fraction (a) with mixing particles and (b) without mixing particles.

geometry studied in the present simulations, as shown in Figure 12. The reactor is made from a Plexiglas cylinder with an inner diameter of 0.08 m, thickness of 0.003 m and a total high of 0.965 m. The reactor is filled with spherical acrylic particles with a diameter of 0.005 m. A gas orifice with an inner diameter of 0.002 m is installed

at the center of the bottom plate for the injection and uniform distribution of the gas phase. Bubbles with a diameter of 0.002–0.003 m are produced. All measurements are accomplished at atmospheric pressure and room temperature. Each experimental run starts by filling the column with the appropriate liquid phase. The experiments are performed with and without mixing particles. For the gas phase, a high-speed digital video camera is used to identify the bubbles and measure relevant bubble characteristics, such as the diameter, velocity, and trajectories. The bubble gas velocity and volume fraction is measured in the radial direction from wall to wall and vertically from the gas inlet, respectively using Photron FASTCAM Viewer software (PFV) Ver. 3282. Figure 13 presents the experimental and simulation results at certain points for air velocity and air volume fraction with and without mixing particles. The observed change in velocities are in good agreement with the CFD results with a deviation of only 5–10%.

6 Conclusions

The CFD simulation using ANSYS Fluent and Eulerian model (k–ε turbulence effect) was implemented. A mesh-independent analysis indicates that the mesh size of 0.002 is sufficient for this study. A quasi-steady state was attained after only 20 s of flow without mixing particles, which indicates that the reactor conical design improves the circulation of gas spreading through the liquid phase. The mixing particles significantly contribute to decreasing the stagnant zones near the walls due to their rotational and vibrational motions. With the help of mixing particles, gas is properly distributed into the reactor; its velocity as well as liquid velocity decreased according to the resistances associated with particles motion. This decrease in gas velocity increases the gas residence time and hold-up inside the reactor that improves the mass and heat transfer between phases and accordingly improves the desired reaction efficiency. The models and results presented in this work will provide a useful basis for further study on the modeling of this novel reactor. The progress in CFD will continue with the development of 3-D simulation to investigate the relation between flow patterns and design. Parametric sensitivity analysis will be carried out to study the effect of various process parameters such velocity (m/s), orifice diameter (m), gas head over liquid (m), diameter of mixing particles (m), and mass flow rate of mixing particle (kg/s) on the air velocity, air volume fraction, total density, eddy viscosity and water velocity. In addition, the effect of mesh size needs to be investigated further. Finer mesh size will bring out further details in the flow structure, which is of great interest. Such an approach has obvious potential for improving the design, scale-up and operation of industrial bubble column reactors and will be the focus of our future work.

Acknowledgments: The authors would like to acknowledge the financial support provided by ADNOC Refining Research Center, Abu Dhabi, UAE. The authors would also like to thank Eng. Abeer Fuad from Architectural Engineering Department and Eng. Amin Safi and Eng. Zahid Qureshi from Mechanical Engineering Department at the UAE University for their help.

Author contribution: All the authors have accepted responsibility for the entire content of this submitted manuscript and approved submission.

Research funding: Abu Dhabi National Oil Company, Refining Research Center, Abu Dhabi, UAE (Grant no. 21N224). https://dx.doi.org/10.13039/501100002672.

Conflict of interest statement: The authors declare no conflicts of interest regarding this article.

References

Anderson, T. B., and R. Jackson. 1967. “Fluid Mechanical Description of Fluidized Beds. Equations of Motion.” *Industrial & Engineering Chemistry Fundamentals* 6: 527–39.

Buwa, V. V., and V. Ranade. 2002. “Dynamics of Gas Liquid Flow in a Rectangular Bubble Column: Experiments and Single /Multi-Group CFD Simulations.” *Chemical Engineering Science* 57: 4715–6.

Charpentier, J.C. 1981. “Mass-Transfer Rates in Gas-Liquid Absorbers and Reactors”, In *Advances in Chemical Engineering*. edited by G. R. C. J. W. H. A. T. V. Thomas, and B. Drew, 1–133. Massachusetts: Academic Press.

Dhotre, M. T., and K. Ekambara. 2004. “CFD Simulation of Sparger Design and Height to Diameter Ratio on Gas Holdup Profiles in Bubble Column Reactors.” *Experimental Thermal and Fluid Science* 28: 407–42.

Dhotre, M. T., K. Ekambara, and J. B. Joshi. 2004. “CFD Simulation of Sparger Design and Height to Diameter Ratio on Gas Hold-Up Profiles in Bubble Column Reactors.” *Experimental Thermal and Fluid Science* 28: 407–21.

El-Naas, M. H. 2017. “System for Contacting Gases and Liquids.” US Patent 9,724,639 B2.

El-Naas, M. H., A. F. Mohammad, M. I. Suleiman, M. Al Musharfy, and A. H. Al-Marzouqi. 2017. “Evaluation of a Novel Gas-Liquid Contactor/Reactor System for Natural Gas Applications.” *Journal of Natural Gas Science and Engineering* 39: 133–42.

Gemello, L., V. cappello, F. Augier, D. Marchisio, and C. Plais. 2018. “CFD-Based Scale-Up of Hydrodynamics and Mixing in Bubble Columns.” *Chemical Engineering Research and Design*, 136: 846–58.

Ibrahim, M. H., M. H. El-Naas, R. Zevenhoven, and S . A. Al-Sobhi. 2019. “Enhanced CO2 Capture Through Reaction With Steel-

Making Dust in High Salinity Water." *International Journal of Greenhouse Gas Control* 91: 102819.

Kartushinsky, A., S. Tisler, J. L. G. Oliveria, and C. W. M. van der Geld. 2016. "Eulerian-Eulerian Modelling of Particle-Laden Two-Phase Flow." *Powder Technology* 301: 999–1007.

Lemoine, R., A. Behkish, L. Sehabiague, Y. J. Heintz, R. Oukaci, and B. Morsi. 2008. "An Algorithm for Predicting the Hydrodynamic and Mass Transfer Parameters in Bubble Column and Slurry Bubble Column Reactors." *Fuel Processing Technology*, 89: 322–43.

Li, G., X. Yang, and G. Dai. 2009, "CFD Simulation of Effects of the Configuration of Gas Distributors on Gas–Liquid Flow and Mixing in a Bubble Column." *Chemical Engineering Science* 64: 5104–16.

Li, Z., X. Guan, L. Wang, Y. Cheng, and X. Li. 2016. "Experimental and Numerical Investigations of Scale-Up Effects on the Hydrodynamics of Slurry Bubble Columns." *Chinese Journal of Chemical Engineering* 24: 967–71.

McClure, D. D., N. Aboudha, J. M. Kavanagh, D. F. Fletcher, and G. W. Barton. 2015. "Mixing in Bubble Column Reactors: Experimental Study and CFD Modeling." *Chemical Engineering Journal* 264: 291–301.

Patankar, S. V. 1980. *Numerical Heat Transfer and Two-Phase Yow*. Washington, DC: Hemisphere.

Pfleger, D., and S. Becker. 2001. "Modelling and Simulation of the Dynamic Flow Behavior in a Bubble Column." *Chemical Engineering Science* 56: 1737–47.

Pfleger, D., and S. Gomes. 1999. "Hydrodynamic Simulations of Laboratory Scale Bubble Columns Fundamental Studies of the Eulerian-Eulerian Modeling Approach." *Chemical Engineering Science* 54: 5091–9.

Pfleger, D., S. Gomes, N. Gilbert, and H.G. Wagner. 1999. "Hydrodynamic Simulations of Laboratory Scale Bubble Columns Fundamental Studies of the Eulerian–Eulerian Modelling Approach." *Chemical Engineering Science* 54: 5091–9.

Pourtousi, M., J. N. Sahu, and P. Ganesan. 2014. "Effect of Interfacial Forces and Turbulence Models on Predicting Flow Pattern Inside the Bubble Column." *Chemical Engineering and Processing: Process Intensification* 75: 38–47.

Sanyal, J., S. Vásquez, S. Roy, and M. P. Dudukovic. 1999. "Numerical Simulation of Gas–Liquid Dynamics in Cylindrical Bubble Column Reactors." *Chemical Engineering Science* 54: 5071–83.

Zhang, D. 2007. *Eulerian Modeling of Reactive Gas-Liquid Flow in a Bubble Column*. Enschede: University of Twente.

Zhang, Z., C. Yang, Y. Zhang, H. Zhu. 2018. "Dynamic Modeling Method for Infrared Smoke Based on Enhanced Discrete Phase Model." *Infrared Physics & Technology* 89: 315–24.